



Green synthesis of active Fe₂O₃ nanoparticles using *Aloe barbadensis* and *Camellia sinensis* for efficient degradation of malachite green and Congo red dye

Zubia Anwer¹ · Abdul Rauf Jamali¹ · Waseem Khan¹ · Jahanzeb Bhatti¹ · Faheem Akhter² · Madhia Batool³

Received: 7 August 2022 / Revised: 30 November 2022 / Accepted: 1 December 2022

© The Author(s), under exclusive licence to Springer-Verlag GmbH Germany, part of Springer Nature 2022

Abstract

The synthesis of metal oxide nanoparticles has gained much attention due to its wide range of applications in the field of industrial, chemical, and biological applications. These metallic nanoparticles have been developed for azo-dye removal, but they are limited for ecofriendly and cost-effective processes. The main objective of this study is to focus on the synthesis of Fe₂O₃-nanoparticles by green route followed by its application in the dye removal process from wastewater. In this approach, the active iron oxide nanoparticles (Fe₂O₃-NPs) were produced successfully using *Camellia sinensis* and *Aloe barbadensis* leaf extract. The prepared nanoparticles were characterized using SEM, XRD, FTIR, and UV–Vis spectroscopy. As per results, the NPs effectively degraded both the azo-dyes from the aqueous solution with 70–80% removal efficiency in 40–45 min under optimum conditions. Moreover, the color change in the solution indicated the formation of Fe₂O₃-NPs. The absorption peak was observed at 275 nm and 270 nm for *Aloe barbadensis* leaf extract and *Camellia sinensis* extract, respectively. The FTIR peak at 553.63 cm⁻¹ indicates the presence of Fe₂O₃ NPs along with other peaks at 2853.3 cm⁻¹ for O–H stretching in carboxylic acid; at 3404 cm⁻¹ due to the O–H group present in the extract, broad peak of 3406 cm⁻¹ shows –OH group of carbohydrates and phenols along with a peak at 2891 cm⁻¹ for asymmetrical and symmetrical C–H stretching. The results of XRD and SEM indicate the homogeneity, shape, and size of NPs, which were spherical and cubic. The size of the particles ranged between 80 and 100 nm for both types of NPs prepared using the extracts. The Langmuir and Elovich isotherms were used to analyze adsorption behavior. The pseudo-first-order and pseudo-second-order kinetic approaches were used and found satisfactory for both approaches. An extensive discussion has been made in light of the experimental data and results obtained.

Keywords *Aloe barbadensis* · *Camellia sinensis* · Iron oxide nanoparticles (Fe₂O₃-NPs) · Green synthesis · XRD · Langmuir isotherm · Elovich isotherm · Pseudo-first-order kinetic study

✉ Faheem Akhter
faheemakhtar86@quest.edu.pk

¹ Department of Materials and Metallurgical Engineering, NED University of Engineering and Technology, Karachi, Pakistan

² Department of Chemical Engineering, Quaid-e-Awam University of Engineering, Science and Technology, Nawabshah, Pakistan

³ Department of Chemistry, Government College University Lahore, Lahore, Pakistan

1 Introduction

Recent scientific and technological advances, particularly in nanotechnology, have resulted in unveiling more methods for synthesizing nanoparticles [1, 2]. Because of the vast number of dyes, detergents, and pigments used in the textile industry, there has been a concerted effort to develop suitable technology for the removal of industrial effluents. It is now possible to follow nanoparticle (NP) synthesis techniques that use fewer costly chemicals, are less harsh on reaction conditions, and are environmentally friendly [3]. Due to their ability to remove organic and inorganic contaminants from water, iron nanoparticles (Fe₂O₃ NPs) have piqued the interest of researchers in recent years [4–6]. Nanotechnology is a discipline of science concerned with altering materials at small scales. Metallic NPs

may be synthesized using both chemical and physical methods. However, these approaches carry drawbacks, such as the use of harmful substances and their effect on the environment. Hence, to deal with this problem, green chemistry research in nanotechnology has become the targeted focus recently [7–9]. To enhance adsorption qualities, the surface area and mass ratios must be increased. As a result, numerous researchers were pushed to create green chemistry and bioprocesses to manufacture NPs that were clean, reliable, biocompatible, benign, and environmentally friendly [10–13]. The use of green synthesis has resulted in the production of exceptionally stable NPs even though it is challenging to keep NPs intact during green synthesis.

Aloe barbadensis juice is widely known for its calming properties. This medication is often used with ointment for skin burns and abrasions. The therapeutic properties of this ancient plant may be even stronger today [14]. *Aloe barbadensis*'s anti-aging properties are well known, and it is often utilized in cosmetics. Those who follow natural health profiles have long regarded these veggies as strong superfoods [15]. *Aloe barbadensis* is high in antioxidant vitamins A and C, as well as B12, folic acid, and choline, among other nutrients. Among the eight enzymes revealed by this molecule are catalase, alkaline phosphatase, amylase, and cellulose. Calcium, copper, selenium, chromium, manganese, magnesium, potassium, and zinc are among the minerals contained in *Aloe barbadensis*. Because of its antioxidant characteristics, *Camellia sinensis* is a well-known nutraceutical. This dish is loaded with antioxidants and nutrients [16]. Tea contains anti-inflammatory and cancer-fighting polyphenols. Caffeine is present in *Camellia sinensis*. This product also contains the amino acid L-theanine, which has the ability to pass the blood–brain barrier.

In the present work, Fe_2O_3 nanoparticles were synthesized using *Camellia sinensis* and *Aloe barbadensis* leaf extract along with their comparative study [17]. A green, sustainable and facile approach was followed. The prepared NPs were then analyzed for their dye removal efficiency, which reached up to 80% under optimum conditions. The manufacture of green Fe_2O_3 nanoparticles is a quick, low-cost, and efficient process. Because of its remarkable structural, electrical, and optical features, NP synthesis has recently gained attention. They may alter their looks as they mature. To lessen the environmental impact, a green synthesis process must be developed [18]. Moreover, the kinetic study was made to study the correlation between the adsorption of the azo dyes in the presence of Fe_2O_3 -nanoparticles.

2 Material and methods

2.1 Materials

All the chemicals used in this study were of analytical grade with 99% purity and purchased from Sigma-Aldrich. The

Camellia sinensis leaves were bought from a commercial tea vendor while *Aloe barbadensis* leaves were obtained from nearby botanical garden of Karachi University.

2.2 Synthesis of Fe_2O_3 -NPs by *Aloe barbadensis* leaf extract

2.2.1 Preparation of extract

The *Aloe barbadensis* leaves were collected from the botanical garden. The plant materials were washed several times with deionized water to remove adhering dirt and impurities and dried. The dried leaves were cut into small pieces, dissolved in 250 ml of deionized water, and heated at 60°C for 15 min. The collected extract was stored at 6°C for further use.

2.2.2 Synthesis of Fe_2O_3 -NPs

Iron chloride ($\text{FeCl}_3 \cdot 6\text{H}_2\text{O}$) was used as a precursor. A 0.01 M $\text{FeCl}_3 \cdot 6\text{H}_2\text{O}$ black solution was added to *Aloe barbadensis* leaf extract in the ratio of 1:1 proportion. Fe_2O_3 -NPs were formed almost immediately after heating the mixture for 20 min at 80 °C. To separate the NPs, the mixture was centrifuged, ethanol washed numerous times, filtered, and dried under vacuum at 40 °C. *Aloe barbadensis* leaves have the greatest potential for ferric chloride reduction when treated with ferric chloride salt. The NP formulation was validated by the external color change from evolving pale orange to dark red.

2.3 Synthesis of Fe_2O_3 -NPs using *Camellia sinensis* extract

2.3.1 Preparation of extract

Fe_2O_3 -NPs were synthesized using *Camellia sinensis* leaves obtained from a local tea vendor, i.e., Tapal Tea. The extract of *Camellia sinensis* was prepared by stringing 30 g of tea in 1000 ml deionized water at 70°C for 20 min. The solution was then filtered, cooled, and stored at 6°C for the synthesis of Fe_2O_3 -NPs.

2.3.2 Fe_2O_3 -NPs synthesis

Iron chloride ($\text{FeCl}_3 \cdot 6\text{H}_2\text{O}$) was used as a precursor. A 0.01 M $\text{FeCl}_3 \cdot 6\text{H}_2\text{O}$ black solution was added to *Camellia sinensis* leaf extract in a ratio of 1:1 proportion. 30 min of stirring at room temperature produced a colloidal suspension. The mixture was then centrifuged and rinsed many times with ethanol before being dried at 40 °C in a vacuum. The formulation of NPs was validated by an exterior color shift from light yellow to black.

2.4 Characterization techniques

Scanning electron microscope (JSM-6480) was used to analyze the particle size, surface morphology, and shape of Fe_2O_3 -NPs. X-ray diffractometer (XRD) was used to analyze the structure of NPs. The adsorption spectrum of prepared Fe_2O_3 -NPs was observed with the help of UV–Vis spectrophotometer (Spectrumlab 22PC, Shanghai; Lengguang Technology Co. Ltd., Shanghai, China).

3 Results and discussion

3.1 Color change

The color change indicates the formation of Fe_2O_3 -NPs. The pale-orange color was turned into dark red for *Aloe barbadensis* extract [19], while the pale-yellow color turned into dark black using *Camellia sinensis* indicating the formation of Fe_2O_3 -NPs [20] as shown in Figs. 1 and 2, respectively. This color change for both *Aloe barbadensis* and *Camellia sinensis* extract is arising from the metabolic chemical reaction of an extract with precursor.

3.2 XRD results

Figure 1 shows the XRD results of Fe_2O_3 -NPs synthesized via *Aloe barbadensis* and *Camellia sinensis* extracts (XPERT-PRO). The obtained data matched with the reference of JCPDS card No. (024–0074). In Fig. 1a, the XRD spectrum shows different diffraction peaks for Fe_2O_3 from *Camellia sinensis* having 2θ values of 24, 33, 35, 41, 49, and 54 corresponding to the crystal planes of [012], [104], [110], [113], [024], and [116], respectively. In Fig. 1b, the diffraction peaks for Fe_2O_3 from *Aloe barbadensis* extract having 2θ values of 35.5 and 62.5 correspond to a crystal plane of [110] and [214], respectively, which show the appearance of Fe_2O_3 -NPs at different crystal planes synthesized using *Aloe barbadensis* extract.

respectively. In Fig. 1b, the diffraction peaks for Fe_2O_3 from *Aloe barbadensis* extract having 2θ values of 35.5 and 62.5 correspond to a crystal plane of [110] and [214], respectively, which show the appearance of Fe_2O_3 -NPs at different crystal planes synthesized using *Aloe barbadensis* extract.

3.3 SEM results

Figure 2 shows the surface morphology and average particle size of Fe_2O_3 oxide nanoparticles analyzed under SEM model (JSM-6480) at different magnifications. As shown in Fig. 4A–C, Fe_2O_3 -NPs obtained using *Camellia sinensis* extract, the particles are spherical and cubic. It can be seen in Fig. 4A–C that the Fe_2O_3 -NPs are more agglomerated rather than uniformly distributed. The average particle size for Fe_2O_3 nanoparticles was around 60–80 nm. On the other hand, the iron oxide nanoparticles obtained using *Aloe barbadensis* (Fig. 4D–F) were spherical and circular. The cubic size of these particles ranged between 80 and 100 nm.

3.4 FTIR analysis

In the present study, FT-IR spectrum was analyzed to confirm Fe_2O_3 NPs. As shown in Fig. 3, the peak at 553.63 indicated the formation of Fe_2O_3 -NPs. The O–H stretch in carboxylic acid appears at 2853.3 cm^{-1} . The band at 3404 cm^{-1} is due to stretching vibrations of O–H groups in water, alcohol, and phenols. The broad peak exhibited at 3406 cm^{-1} indicates the stretching of the -OH group of phenol and carbohydrate monomers which includes mannose and uranic acid. The peak at 2891 cm^{-1} was assigned for asymmetrical and symmetrical C–H stretching of aliphatic -CH₂ and -CH groups.

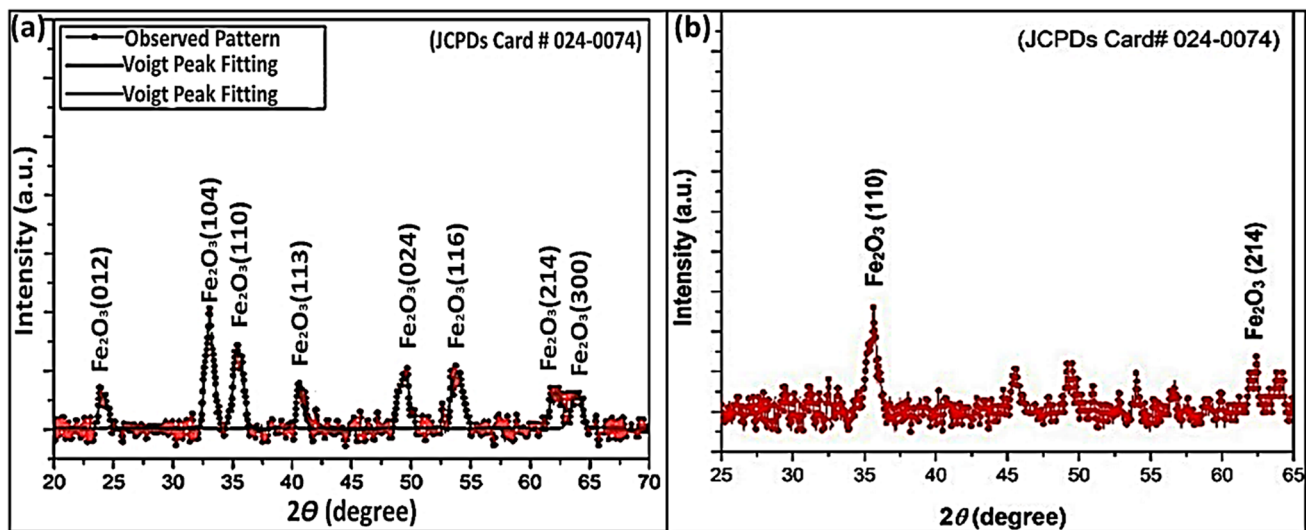


Fig. 1 XRD results of Fe_2O_3 -NPs: a *Camellia sinensis* extract, b *Aloe barbadensis* extract

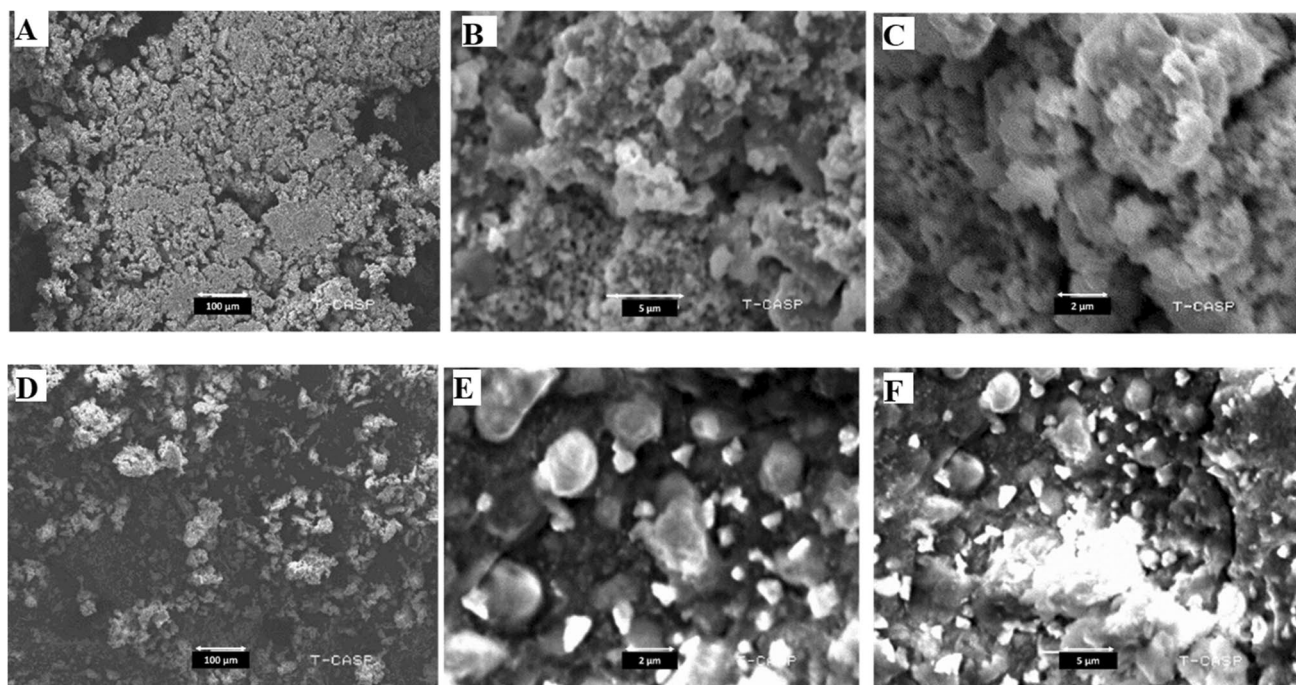
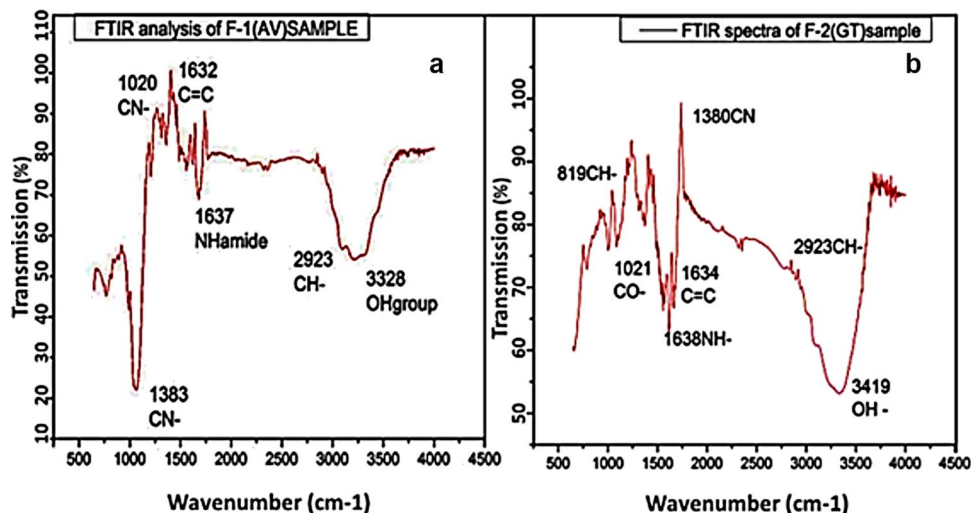


Fig. 2 SEM Images for Fe_2O_3 NPs obtained using *Camellia sinensis* extract (A, B, C); Fe_2O_3 NPs obtained using *Aloe barbadensis* leaf extract (D, E, F)

Fig. 3 Functional groups present in iron oxide nanoparticles. **a** *Aloe barbadensis*; **b** *Camellia sinensis*



3.5 UV–vis spectrophotometer

Figure 4 shows the absorption peak of Fe_2O_3 -NPs synthesized by tea and *Aloe barbadensis* extract. It can be observed that the absorption peaks of UV–vis spectroscopy range from 270 to 300 nm which confirms the formation of Fe_2O_3 -NPs [20]. The UV–vis range of Fe_2O_3 -NPs is at 275 nm occurring using *Aloe barbadensis* leaf extract, whereas the absorption range of Fe_2O_3 -NPs is at 270 nm by using *Camellia sinensis* extract. The mechanism of light-matter interaction was used in which the Fe_2O_3 -NPs absorb the ultraviolet radiation, hence producing

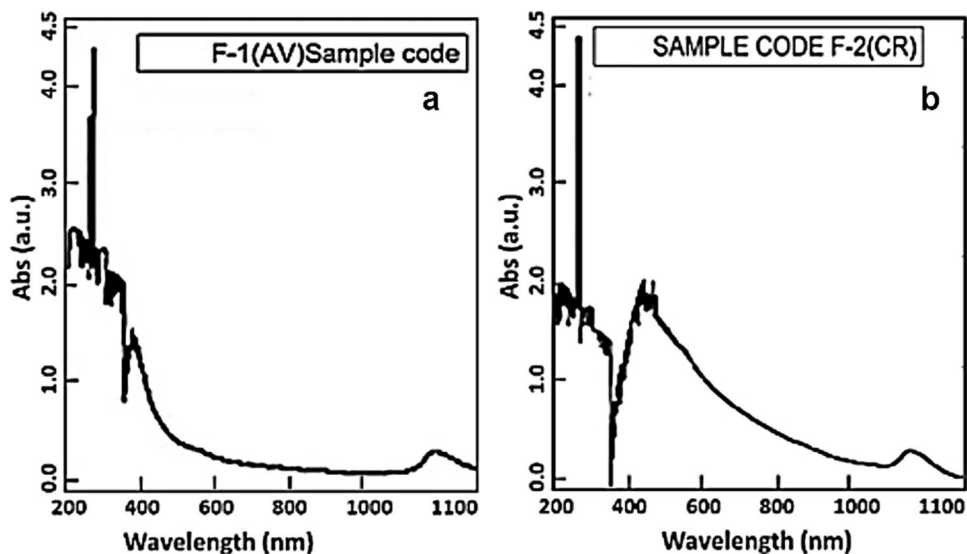
distinct spectra. As per the statement of Beer-Lambert's law, the greater the concentration of absorbing molecules in a solution, the greater will be the absorption of radiations [21].

3.6 Effect of parameters on azo-dye removal using Fe_2O_3 -NPs

3.6.1 Effect of time

A UV–vis spectroscopy was used to investigate the effect of time on the proportion of azo-dyes that degraded. Figure 5a and

Fig. 4 UV–vis images of iron oxide nanoparticles. **a** *Aloe barbadensis* and **b** *Camellia sinensis*



b demonstrates *Aloe barbadensis* and *Camellia sinensis* F-1 and F-2 examples of iron oxide NPs generated (A.V. and GT). All samples required between 40 and 45 min to remove the azo dye at a rate of 75 to 80%. The graphs demonstrate that the degradation of azo dyes malachite green-MG and acid red 28-CR with adsorbent Fe₂O₃-NPs is time-dependent. The temperature and initial concentration were kept constant throughout the experiment at 308 Kelvin and 20–250 mg/l, respectively.

3.6.2 Effect of pH

The influence of pH on the removal of Congo red and malachite green azo dyes was investigated using a UV–vis spectroscope (Fig. 6). The degradation rate of azo dyes was

determined experimentally throughout a pH range (2–14). For samples F-1 and F-2, the maximum rate of Congo red dye degradation was reported at a pH of 5. Malachite green, on the other hand, showed the greatest deterioration at pH 4. This implies that the optimal pH for removing both dyes is between 4 and 5, respectively. In addition, the graph demonstrates that dye removal is effective when the pH is acidic, but the degradation rate reduces dramatically when the pH approaches basicity.

3.6.3 Effect of temperature

The temperature affects percentage degradation effectually. The observed results (Fig. 7) indicate that after

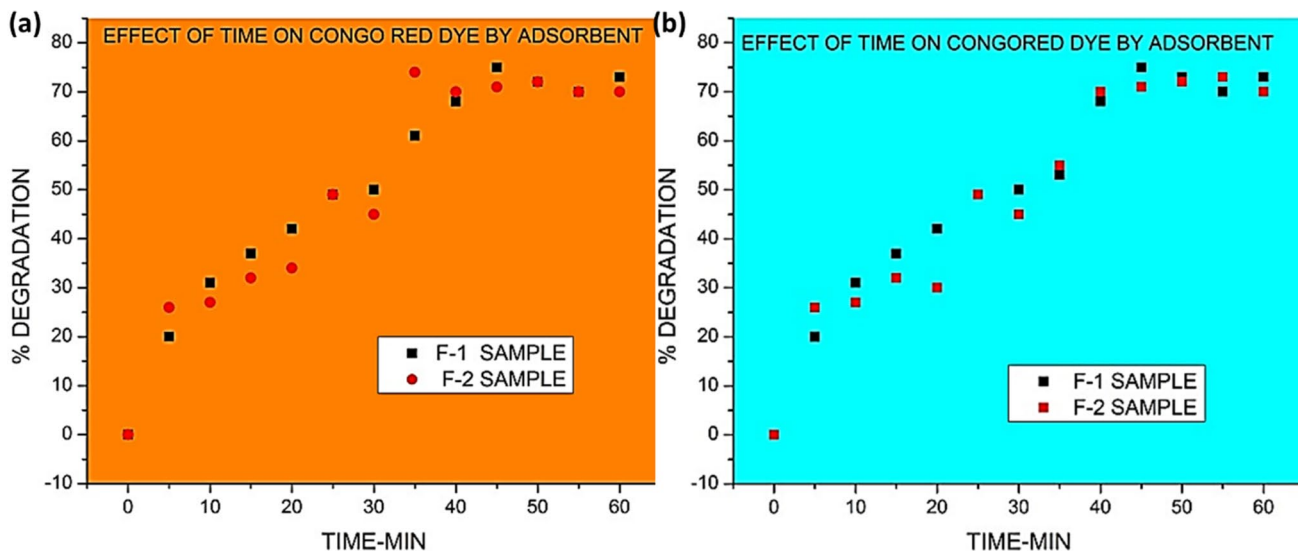


Fig. 5 **a** Effect of time by Fe₂O₃-NPs samples F-1 and F-2 (AV, GT) on Congo red dye calculated by ultraviolet spectrometer DB-20. **b** Effect of time by Fe₂O₃-NPs samples F-1 and F-2 (AV, GT) on malachite green dye calculated by ultraviolet spectrophotometer DB-20

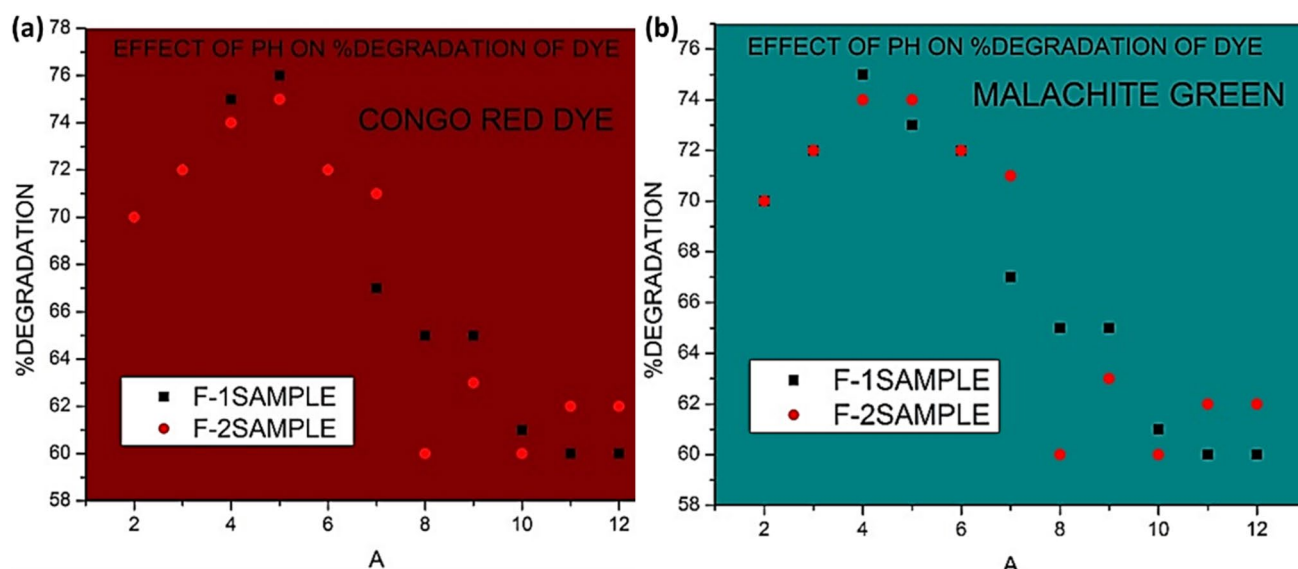


Fig. 6 **a** Effect of pH by Fe_2O_3 -NPs sample F-1 and F-2 (synthesized by *Aloe barbadensis* and *Camellia sinensis* extract) on Congo red dye calculated by ultraviolet spectrophotometer DB-20. **b** Effect of pH by

Fe_2O_3 -NPs sample F-1 and F-2 (synthesized by *Aloe-barbadensis* and *Camellia sinensis* extract) on malachite green dye calculated by ultraviolet spectrophotometer DB-20

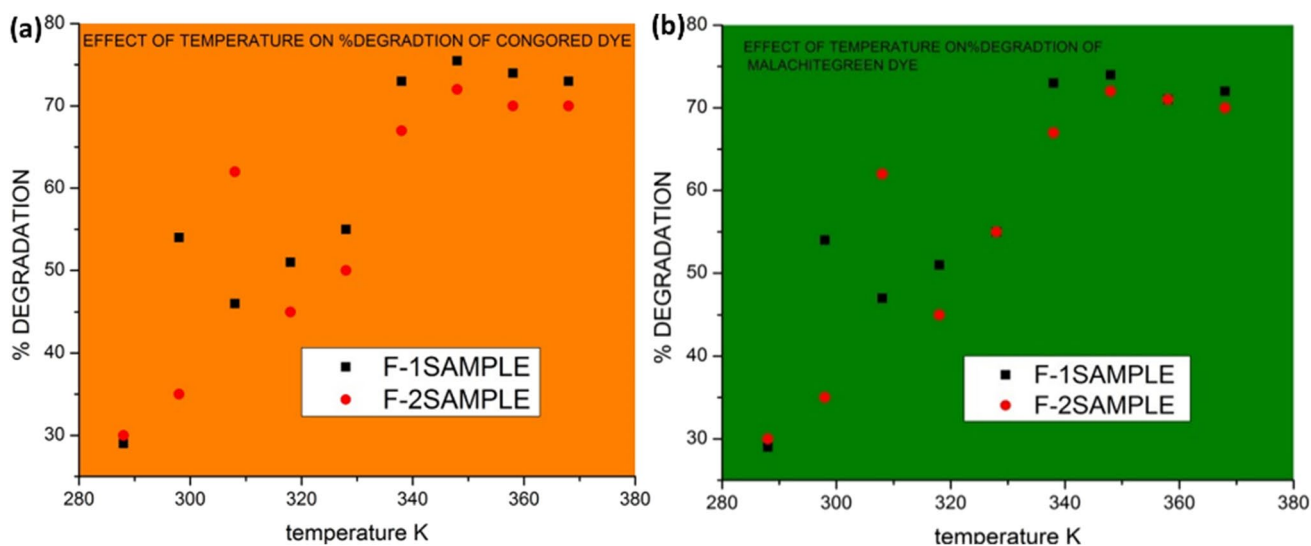


Fig. 7 **a** Effect of temperature by Fe_2O_3 -NPs sample F-1 and F-2 on Congo red dye calculated by ultraviolet spectrophotometer DB-20. **b** Effect of temperature by Fe_2O_3 -NPs sample F-1 and F-2 on malachite green dye calculated by ultraviolet spectrophotometer DB-20

increasing temperature from 320 to 360 K, the percentage removal potential of Fe_2O_3 -NPs samples F-1 and F-2, i.e., green synthesized by *Aloe barbadensis* and *Camellia sinensis*, respectively, increases significantly. For Congo dye, the highest removal was achieved at a temperature 340 K (F-1, F-2), whereas for Malachite Green, it was 350 K, respectively. For both the dyes, the removal efficiency of nanoparticles significantly improved when the temperature increased from 320 K.

Hence, the optimum temperature range for nanoparticles to remove the dyes was found to be between 330 and 350 K, respectively.

3.7 Adsorption kinetic studies

The kinetic study of azo dye adsorption was done using optimum conditions. The kinetic parameters are useful for the analysis of the adsorption rate. A relationship between

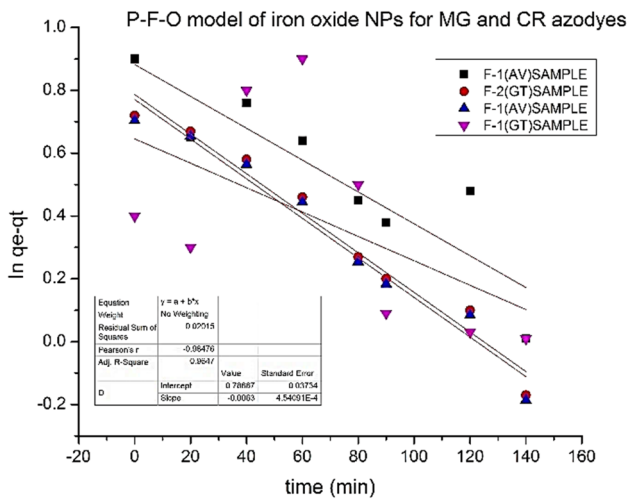


Fig. 8 PFO model of iron oxide NPs

different parameters was observed for linearity. The rate constant was calculated using a graph, and constants were calculated from adsorption kinetic models at 35 °C.

3.7.1 Pseudo-first-order kinetic models of Fe₂O₃-NPs

P-F-O model (Lagergren kinetic model) is the most experimented kinetic model for explaining the solute adsorption in solution (Fig. 8). The expression is given below:

$$\ln(q_e - q_t) = \ln q_e - K_1 t \quad (1)$$

where q_e , q_t is the amount of adsorbent NPs and nanocomposites, t is time, and k_1 is the constant of P-F-O adsorption. When this equation is applied to experimental data between $\ln(q_e - q_t)$ versus time, the straight line proves that the model fits best for adsorption.

3.7.2 Pseudo-second-order kinetic model of Fe₂O₃-NPs

From the readings of R^2 for pseudo-first-order and pseudo-second-order, it was concluded that the pseudo-second-order model provides a better correlation. The R^2 value from the graph for pseudo-second-order kinetics of CR and MG was 0.997, 0.99, 0.998, and 0.989 for F-1 and F-2 samples synthesized via *Aloe barbadensis* and *Camellia sinensis* leaf

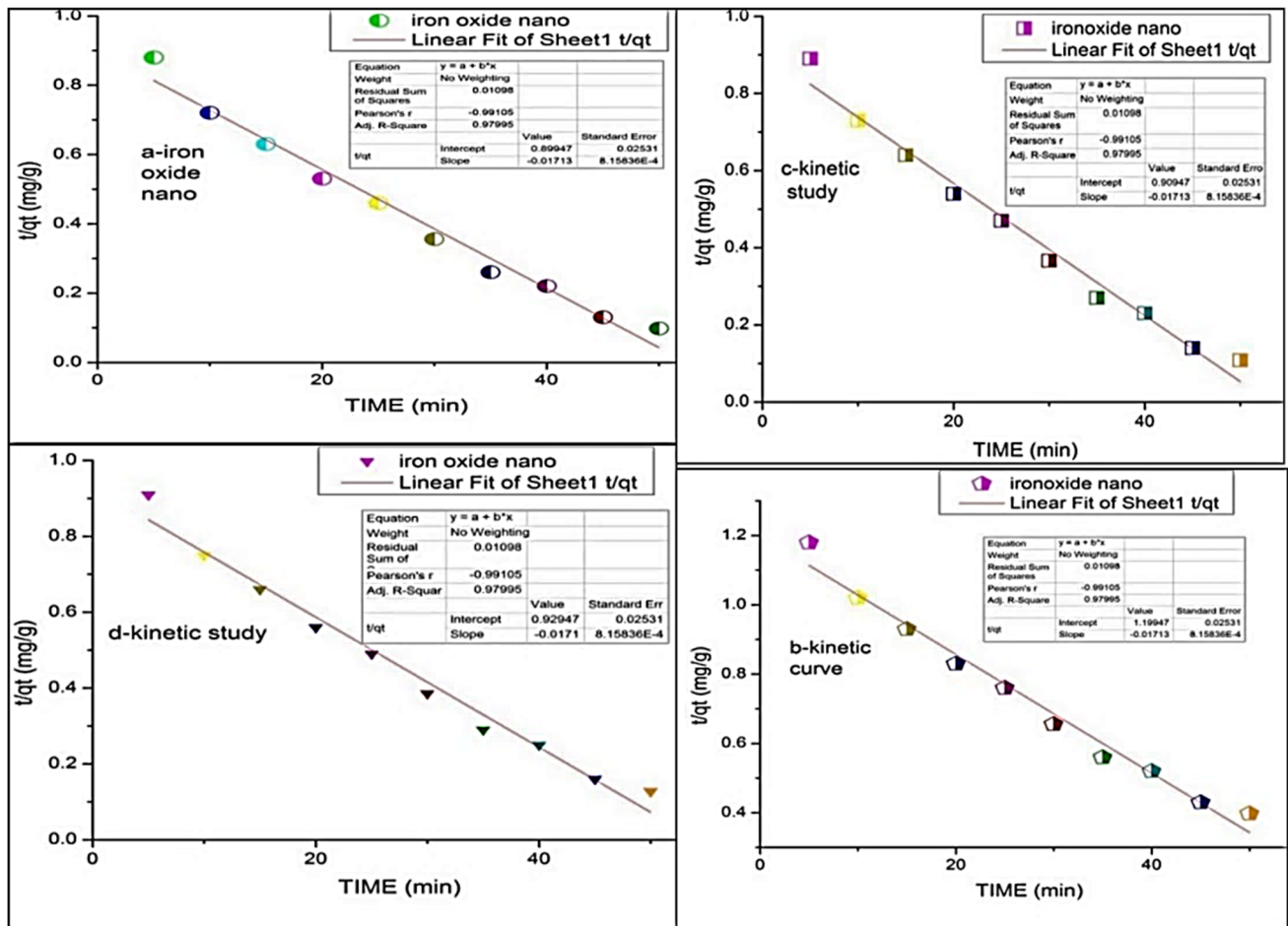


Fig. 9 Kinetic study of pseudo-first-order and pseudo-second-order

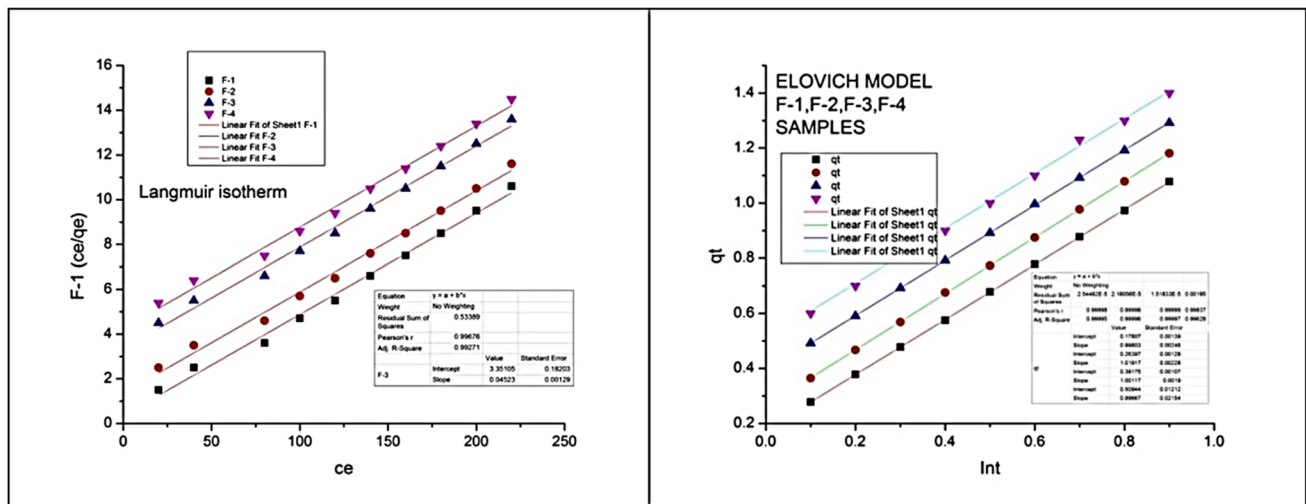


Fig. 10 Adsorption isotherms

extracts, respectively, at an optimum temperature of 35 °C. This high value indicates that adsorption of colored and malachite green dye onto adsorbent follows a pseudo-second-order model of kinetics (Fig. 9).

3.8 Adsorption isotherm models

The experimental adsorption kinetic data was judged by using reaction adsorption models Langmuir adsorption isotherm and Elovich adsorption models based on the assumptions that the adsorption mechanism is based on chemical reactions that are responsible for absorption. The Langmuir isotherm relies on the assumption that there is no lateral interaction, but the reactive groups species are homogeneously distributed to the surface of the particulate. The results are listed below in graphical form to confirm the applicability of these models for linearity (Fig. 10).

4 Conclusion

The green synthesized Fe_2O_3 nanoparticles are cost-effective biogenic molecules with the ability to serve as dye adsorbents. The current study has shown the effective synthesis of iron oxide nanoparticles with an average particle size between 80 and 100 nm using leaf extracts of *Aloe barbadensis* plant and *Camellia sinensis*. Moreover, an extensive study has been made for the removal of azo dyes using Fe_2O_3 nanoparticles. Contact time, pH, and temperature were the parameters that affected the adsorption phenomena and were found satisfactory for this study. A time-dependent adsorption criterion was

observed. About 70–80% of azo dye removal, i.e., azo dyes malachite green-MG and acid red 28-CR with Fe_2O_3 NPs as adsorbent, has been achieved in 40–45 min under optimum conditions. Moreover, the pseudo-second-order kinetic model fitted best with experimental data on dye removal with an R^2 value of F-1 and F-2 samples for CR-dye as 0.997 and 0.99, respectively. In addition, the R^2 values for F-1 and F-2 samples for MG-dye as 0.998 and 0.989, respectively.

Acknowledgements Thanks to GCU CASP department for providing SEM, XRD, FT-IR facility.

Author contribution Zubia Anwar, Abdul Rauf Jamali, Waseem Khan: Abstract, introduction, materials and methods. Jahanzeb Bhatti, Faheem Akhter, Madhia Batool, Zubia Anwar: Results and discussion, conclusion. Zubia Anwar: Thorough revision of manuscript by implementing the reviewers' comments.

Data availability The data presented in this work is available with the corresponding author and can be provided on considerable request.

Declarations

Ethics approval and consent to participate Not applicable.

Competing interests The authors declare no competing interests.

References

- Wu F, Misra M, Mohanty AK (2021) Challenges and new opportunities on barrier performance of biodegradable polymers for sustainable packaging. *Prog Polym Sci* 117:101395. <https://doi.org/10.1016/J.PROGPOLYMSCI.2021.101395>
- Salem SS, Badawy MSEM, Al-Askar AA et al (2022) Green biosynthesis of selenium nanoparticles using orange peel waste: characterization, antibacterial and antibiofilm activities against

- multidrug-resistant bacteria. *Life* 12:893. <https://doi.org/10.3390/LIFE12060893>
3. Pereira ADES, Oliveira HC, Fraceto LF, Santaella C (2021) Nanotechnology potential in seed priming for sustainable agriculture. *Nanomaterials* 11:1–29
 4. Polshettiwar V, Varma RS (2010) Green chemistry by nano-catalysis. *Green Chem* 12:743. <https://doi.org/10.1039/b921171c>
 5. Salem SS, Fouda A (2020) Green synthesis of metallic nanoparticles and their prospective biotechnological applications: an overview. *Biol Trace Element Res* 1(199):344–370. <https://doi.org/10.1007/S12011-020-02138-3>
 6. Salem SS (2022) Bio-fabrication of selenium nanoparticles using baker's yeast extract and its antimicrobial efficacy on food borne pathogens. *Appl Biochem Biotechnol* 194(5):1898–1910. <https://doi.org/10.1007/S12010-022-03809-8>
 7. Hunt AJ, Anderson CWN, Bruce N et al (2014) Phytoextraction as a tool for green chemistry. *Green Processing and Synthesis* 3:3–22. <https://doi.org/10.1515/GPS-2013-0103>
 8. Salem SS, Hammad EN, Mohamed AA, El-Dougoudou W (2023) A comprehensive review of nanomaterials: types, synthesis, characterization, and applications. *Review* 13:41. <https://doi.org/10.33263/BRIAC131.041>
 9. Al-Rajhi AMH, Salem SS, Alharbi AA, Abdelghany TM (2022) Ecofriendly synthesis of silver nanoparticles using Kei-apple (*Dovyalis caffra*) fruit and their efficacy against cancer cells and clinical pathogenic microorganisms. *Arab J Chem* 15:103927. <https://doi.org/10.1016/J.ARABJC.2022.103927>
 10. Ndolomingo MJ, Bingwa N, Meijboom R (2020) Review of supported metal nanoparticles: synthesis methodologies, advantages and application as catalysts. *J Mater Sci* 55:6195–6241. <https://doi.org/10.1007/s10853-020-04415-x>
 11. Abdelmoneim HEM, Wassel MA, Elfeky AS et al (2021) Multiple applications of CdS/TiO₂ nanocomposites synthesized via microwave-assisted sol–gel. *J Clust Sci* 33(3):1119–1128. <https://doi.org/10.1007/S10876-021-02041-4>
 12. Shehabeldine AM, Salem SS, Ali OM et al (2022) Multifunctional silver nanoparticles based on chitosan: antibacterial, antibiofilm, antifungal, antioxidant, and wound-healing activities. *J Fungi* 8:612. <https://doi.org/10.3390/JOF8060612>
 13. Salem SS (2022) Baker's yeast-mediated silver nanoparticles: characterisation and antimicrobial biogenic tool for suppressing pathogenic microbes. *BioNanoScience* 2022:1–10. <https://doi.org/10.1007/S12668-022-01026-5>
 14. Morales G, Campillo G, Vélez E et al (2019) Green synthesis of magnetic nanoparticles using leaf extracts of *Aloe vera* and *Kalanchoe daigremontiana* to remove divalent mercury from natural waters. *J Phys Conf Ser* 1247:012021. <https://doi.org/10.1088/1742-6596/1247/1/012021>
 15. Day CM, Sweetman MJ, Hickey SM et al (2021) Concept design, development and preliminary physical and chemical characterization of tamoxifen-guided-mesoporous silica nanoparticles. *Molecules* 26:1. <https://doi.org/10.3390/MOLECULES26010219>
 16. Aidaros N, Mosallam R, Farouk H (2021) Effect of green tea, black tea and moringa oleifera on remineralization of artificially demineralized enamel and dentin: an in-vitro microhardness analysis. *Adv Dental J* 3:24–34
 17. Akhter F, Soomro SA, Siddique M, Ahmed M (2021) Plant and non-plant based polymeric coagulants for wastewater treatment: a review. *J Kejuruteraan* 33:175–181. [https://doi.org/10.17576/jkukm-2021-33\(2\)-02](https://doi.org/10.17576/jkukm-2021-33(2)-02)
 18. Akhter F, Rao AA, Abbasi MN et al (2022) A comprehensive review of synthesis, applications and future prospects for silica nanoparticles (SNPs). *Silicon*. <https://doi.org/10.1007/s12633-021-01611-5>
 19. Gunalan S, Sivaraj R, Venkatesh R (2012) *Aloe barbadensis* Miller mediated green synthesis of mono-disperse copper oxide nanoparticles: optical properties. *Spectrochim Acta A Mol Biomol Spectrosc* 97:1140–1144. <https://doi.org/10.1016/j.saa.2012.07.096>
 20. Paulpandian P, Beevi IS, Somanath B et al (2022) Impact of *Camellia sinensis* iron oxide nanoparticle on growth, hemato-biochemical and antioxidant capacity of blue gourami (*Trichogaster trichopterus*) fingerlings. *Biol Trace Elem Res*. <https://doi.org/10.1007/S12011-022-03145-2>
 21. Picollo M, Aceto M, Vitorino T (2019) UV-Vis spectroscopy. *Physical Sciences Reviews* 4:4. <https://doi.org/10.1515/PSR-2018-0008/MACHINEREADABLECITATION/RIS>

Publisher's note Springer Nature remains neutral with regard to jurisdictional claims in published maps and institutional affiliations.

Springer Nature or its licensor (e.g. a society or other partner) holds exclusive rights to this article under a publishing agreement with the author(s) or other rightsholder(s); author self-archiving of the accepted manuscript version of this article is solely governed by the terms of such publishing agreement and applicable law.